JACS
JOURNAL OF THE AMERICAN CHEMICAL SOCIETY
Communication
pubs.acs.org/JACS

Exceptional Size-Dependent Activity Enhancement in the Electroreduction of CO_2 over Au Nanoparticles

Hemma Mistry,[†] Rulle Reske,[‡] Zhenhua Zeng,[§] Zhi-Jian Zhao,[§] Jeffrey Greeley,[§] Peter Strasser,*[,‡] and Beatriz Roldan Cuenya*[,∥]

[†]Department of Physics, University of Central Florida, Orlando, Florida 32816, United States
[‡]Department of Chemistry, Chemical Engineering Division, Technical University Berlin, 10623 Berlin, Germany
[§]School of Chemical Engineering, Purdue University, West Lafayette, Indiana 47907, United States
[∥]Department of Physics, Ruhr-University Bochum, 44780 Bochum, Germany

Supporting Information

ABSTRACT: The electrocatalytic reduction of CO_2 to industrial chemicals and fuels is a promising pathway to sustainable electrical energy storage and to an artificial carbon cycle, but it is currently hindered by the low energy efficiency and low activity displayed by traditional electrode materials. We report here the size-dependent catalytic activity of micelle-synthesized Au nanoparticles (NPs) in the size range of ∼1−8 nm for the electroreduction of CO_2 to CO in 0.1 M $KHCO_3$. A drastic increase in current density was observed with decreasing NP size, along with a decrease in Faradaic selectivity toward CO. Density functional theory calculations showed that these trends are related to the increase in the number of low-coordinated sites on small NPs, which favor the evolution of H_2 over CO_2 reduction to CO. We show here that the H_2/CO product ratio can be specifically tailored for different industrial processes by tuning the size of the catalyst particles.

Because of the growing global demand for energy, rising CO_2 emissions from the burning of fossil fuels are an increasing environmental threat that, if unmitigated, could have disastrous environmental consequences. An ideal solution would be not only to curb CO_2 emissions by switching to sustainable energy sources but also to capture and reutilize waste CO_2 though its conversion into fuels and valuable chemicals.[1] A promising method of CO_2 utilization is its direct electrocatalytic reduction into useful hydrocarbons, such as methane and ethylene, or H_2 and CO for Fischer−Tropsch processes.[2,3] Several electrochemical[3−7] and computational[6−10] studies have investigated different metal electrodes for this reaction. However, low energy efficiency due to the need for high overpotentials to activate this reaction and low selectivity for desirable hydrocarbons compared with the formation of H_2 mean that this process is not yet industrially viable.[11] Pioneering work by Hori and others demonstrated that gold is one of the few metals that can produce CO from the reduction of CO_2.[4,12,13] Several recent studies indicate that gold electrodes with modified surface morphologies have superior catalytic properties to traditional polycrystalline gold electrodes.[14−16] However, studies of well-defined ligand-free Au NPs in the nanometer size range (<2 nm), where electronic and geometric finite-size effects play a significant role in catalytic activity and selectivity,[17,18] are still missing for this reaction. This study sets out to fill this critical knowledge gap by exploring catalytic size effects in this important size regime.

In order to elucidate the effect of structure on the CO_2 electroreduction reaction over gold, we synthesized monodispersed Au NPs using the inverse micelle encapsulation method followed by complete ligand removal by an O_2 plasma treatment. The catalytic activity and selectivity toward CO formation during the electroreduction of CO_2 over these catalysts were measured and shown to have a striking correlation with NP size. In order to understand these trends, periodic density functional theory (DFT) calculations of Au NPs in the experimentally relevant size range and Au single-crystal surfaces were performed, revealing the relation between surface atomic coordination and catalytic behavior. Our work has uncovered exceptionally high intrinsic catalytic CO_2 electroreduction activities and previously unexplored size-dependent CO and H_2 selectivities that translate to tunable H_2/CO synthesis gas ratios for use in a variety of different subsequent catalytic transformations.

By means of the inverse micelle encapsulation method,[18−21] nine Au NP samples ranging from 1.1 to 7.7 nm in size were prepared and deposited on glassy carbon. The samples are labeled Au1 to Au9 in order of increasing size. For atomic force microscopy (AFM) morphological characterization, the NPs were deposited onto SiO_2/Si(111). Figure 1 shows AFM images of the Au NPs after removal of the polymeric ligands. AFM analysis revealed that the Au NPs had been prepared with narrow size distribution and uniform coverage across the support. Size histograms are shown in Figure S1 in the Supporting Information (SI), and Table S1 lists the synthesis parameters and AFM analysis results for each sample. Additionally, a cross-sectional TEM image of our Au NPs supported on SiO_2/Si(111) was acquired, revealing the spherical shape of our NPs (Figure S2). The relative Au surface coverage for each sample determined from AFM (assuming a spherical NP shape with the measured AFM height and NP density) was used to normalize all of the subsequent electrochemical measurements.

Received: August 28, 2014
Published: October 17, 2014

   dx.doi.org/10.1021/ja508879j | J. Am. Chem. Soc. 2014, 136, 16473−16476

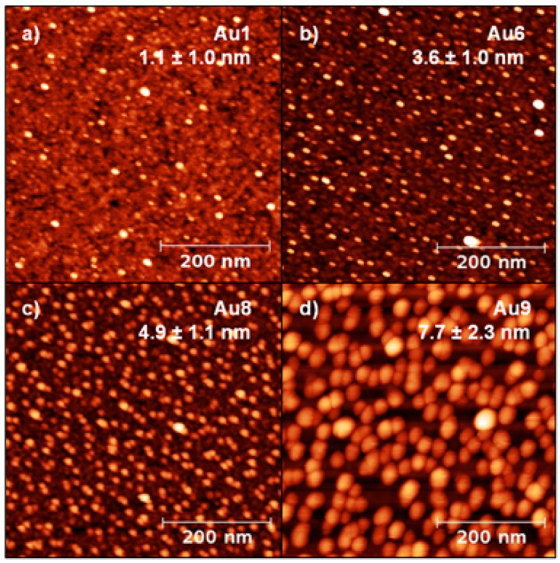

Figure 1. AFM images of four differently sized Au NP samples prepared by inverse micelle encapsulation and supported on SiO_2/Si(111): (a) Au1 (1.1 ± 1.0 nm); (b) Au6 (3.6 ± 1.0 nm); (c) Au8 (4.9 ± 1.1 nm); (d) Au9 (7.7 ± 2.3 nm).

The Au NPs deposited onto glassy carbon supports were used as working electrodes for the electrochemical reduction of CO_2 in 0.1 M $KHCO_3$ at pH 6.8. Linear sweep voltammograms (LSVs) measured from E = +0.22 to −1.22 V vs reversible hydrogen electrode (RHE) are shown in Figure 2a after subtraction of a background signal measured on the glassy carbon support and after normalization by the Au surface area. For clarity, only five of the Au samples are shown here. LSVs of the remaining samples are shown in Figure S3, in addition to that of a Au foil measured under identical conditions. Decreasing the particle size from 7.7 to 1.1 nm resulted in a drastic increase in catalytic activity over a wide range of potentials. Figure 2b shows the current density measured at E = −1.2 V vs RHE as a function of NP size for all of the samples. Strikingly, the smallest NPs in sample Au1 displayed over 100 times the activity of the largest NPs. All samples below 5 nm in size showed significantly higher activity than bulk Au, while the largest NPs, Au8 and Au9, showed comparable activity to bulk gold.

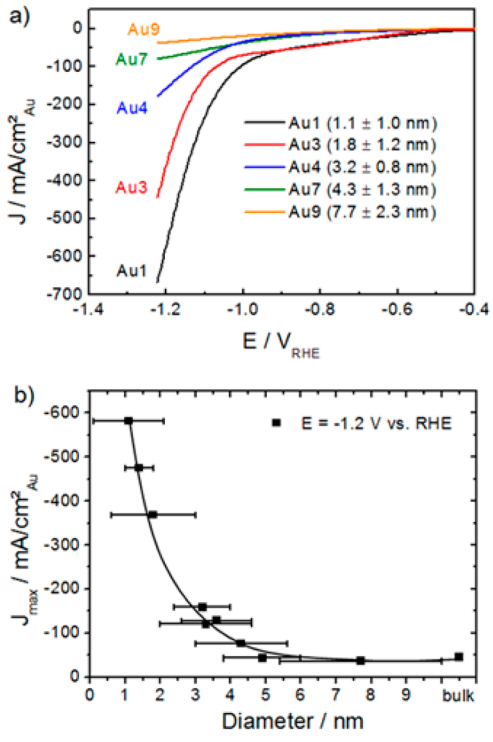

Figure 2. (a) Linear sweep voltammetry of CO_2 electroreduction over Au NP catalyst samples. Data were acquired at room temperature in 0.1 M $KHCO_3$ with a −5 mV/s scan rate and were normalized by the respective Au surface areas after subtraction of a background signal measured on clean glassy carbon. (b) Faradaic current densities at E = −1.2 V vs RHE as a function of Au NP size, with error bars indicating NP size distributions.

The absolute volume percent of reaction products was measured under steady-state reaction conditions at E = −1.22 V vs RHE in order to characterize the NP size effect on the reaction pathways. The results revealed that the increase in activity for small NPs below 5 nm is mainly due to a sharp increase in H_2 production (Figure 3a). Figure 3b shows the Faradaic selectivity as a function of particle size, revealing a clear size effect on the selectivity toward the two reaction products, CO and H_2. While the smallest NPs below 5 nm overwhelmingly favored the production of H_2, the largest NPs (7.7 nm, Au9) showed a sudden increase in selectivity toward CO. The intermediate NP sizes showed an approximately constant Faradaic selectivity toward CO of ∼18%, while Au9 showed the maximum CO selectivity of 45% and Au1 showed a minimum of 9%. Consistent with earlier measurements by Noda[12] and Hori[4,13] (after conversion to the RHE scale; see the SI), a gold foil measured under identical conditions showed 88.6% Faradaic selectivity toward H_2 and 11.4% toward CO at E = −1.22 V vs RHE, so that all NP samples except Au1 displayed higher selectivity toward CO than bulk Au. Evaluation of the actual space time yields of CO revealed that Au1 produces more than 8 mL of CO and over 80 mL of H_2 per hour and square centimeter of active surface, corresponding to more than 0.36 mmol h^{-1} cm^{-2} and 3.6 mmol h^{-1} cm^{-2} CO and H_2, respectively, at the applied cell voltage. The H_2/CO molar ratio produced by each sample is plotted in Figure 3c. Changing the size of the catalyst particle enables careful tuning of the H_2/CO ratio in the product stream to acquire the desired composition. NPs below 5 nm in size produce H_2/CO ratios greater than 3, which is ideal for the methane (synthetic natural gas, SNG) synthesis reaction. Between 5−7.5 nm, a H_2/CO ratio of 2 can be inferred by extrapolation, which is suited for methanol synthesis or Fischer−Tropsch processes. At a H_2/CO ratio of 1, which occurs on NPs approximately 7.5 nm in size, the product stream can be used for hydroformylation of alkenes to aldehydes.

The superior catalytic activity of Au NPs less than 5 nm in size is often explained by the increasing ratio of low-coordinated surface sites such as edges and corners.[17,18] These low-coordinated sites allow for stronger binding of reactants or intermediate species, which can lead to increased activity and changes in product selectivity.[22] In order to investigate the population of such active sites on our NPs, model spherical fcc Au structures between 1 and 20 nm in diameter were generated (see the SI, Figure S4). The population of atoms with CN less than 8 on the NP surface increases significantly for NPs below 2 nm, which is in excellent correlation with the enhanced activity of these NPs shown in Figure 2b.

Cuboctahedral clusters were used as model shapes by Zhu et al.[16] to determine the number of edge and corner sites for given NP sizes in order to establish structure−reactivity correlations.

dx.doi.org/10.1021/ja508879j | J. Am. Chem. Soc. 2014, 136, 16473−16476

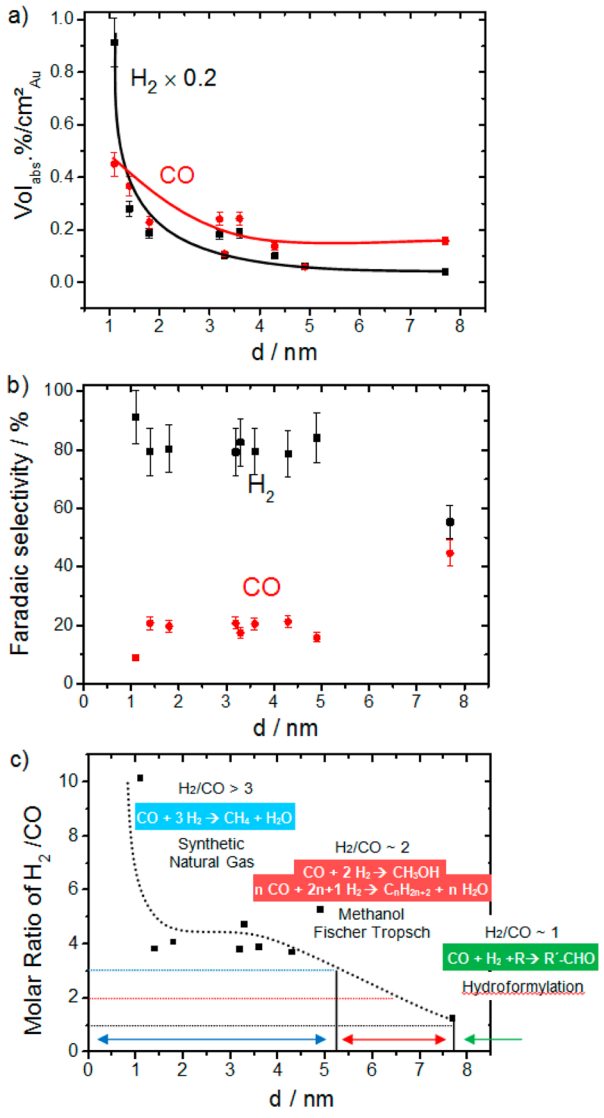

Figure 3. (a) Particle size dependence of the composition of gaseous reaction products (balance is CO_2) during catalytic CO_2 electroreduction over Au NPs. (b) Faradaic selectivity toward H_2 and CO as a function of NP size. Data were acquired in 0.1 M $KHCO_3$ at $E = -1.2$ V vs RHE. (c) Ratio of the volume % of H_2 and CO produced at $E = -1.2$ V vs RHE as a function of NP size.

However, their models fail to account for the difference in activity they observed for NPs between 8 and 10 nm, and no experimental data were available for the most interesting samples, namely, those with sizes below 2−3 nm. As discussed in the SI, it is expected that our NPs are spherically shaped with energetically unfavorable low-coordinated atoms present on the NP surface, as opposed to lower-energy facets. As shown below, our smallest NPs (1.1 nm) were also modeled on the basis of structures obtained by DFT.

Size-dependent reactivity was also observed by Kaufmann et al.[15] for CO_2 electroreduction over ligand-protected $Au_{25}(SC_2H_4Ph)_{18}^-$ clusters (∼1 nm) compared with bare 2 and 5 nm Au NPs and bulk Au. They also found that the current density increases with decreasing particle size, but their catalytic activities were an order of magnitude lower than those presented on the present ligand-free Au NPs. Our smallest NPs in sample Au1 (1.1 nm in size) produced H_2 at a rate of 3.6 mmol h^{-1} cm^{-2} at $E = -1.2$ V vs RHE. In comparison, Kauffman et al. reported a rate of approximately 0.01 mmol h^{-1} cm^{-2} for similarly sized ligand-protected Au_{25} NPs at the same potential. The low efficiency for H_2 production on their ligand-protected NPs could be due to blocking of low-coordinated corner sites by the encapsulating ligands, since such sites are expected to favor H_2 evolution. Regardless, because of the low hydrogen yield, ligand-protected Au NPs appear to be unsuitable for the production of industrially valuable synthesis gas.

To further evaluate the effect of NP size on CO_2 electroreduction, DFT calculations were conducted on several models of both extended Au surfaces and Au NPs, including a Au(111) terrace, a Au(211) step, and Au_{38} and Au_{55} NPs (see the SI for more details). The results at 0 V vs RHE are shown in Figure 4.

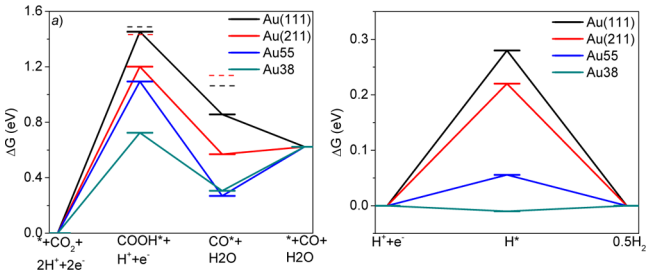

Figure 4. Free energy diagrams for electrochemical reduction of (a) CO_2 to CO and (b) H^+ to H_2 on Au(111) (black lines), Au(211) (red lines), Au_{55} NPs (blue lines), and Au_{38} NPs (cyan lines) at 0 V vs RHE. The dashed lines are results of calculations performed with a full monolayer of adsorbed H.

We see that, consistent with previous calculations,[23] the CO_2 electroreduction intermediates COOH* and CO* are stabilized on both the steps and NPs compared with Au(111). Similar stabilizing trends are seen for the H_2 evolution reaction (HER) intermediate H*, where ΔG (at 0V vs RHE) is reduced from 0.28 eV on Au(111) to 0.21 eV on Au(211) and further to 0.06 and −0.01 eV on Au_{55} and Au_{38} NPs, respectively. Since a good HER catalyst is required to exhibit H* binding that is neither too strong nor too weak, i.e., a ΔG close to 0 V,[24−26] the stabilization of H* on Au NPs implies that Au, a traditionally inert HER catalyst, could actually catalyze this reaction if the NPs are sufficiently small and contain many undercoordinated defects. For the CO_2 electroreduction intermediates, COOH* is stabilized from ΔG = 1.47 eV on Au(111) to 1.27 eV on Au(211) and further to 1.11 and 0.71 eV on Au_{55} and Au_{38}, respectively. These results, calculated at low surface adsorbate coverages, strongly imply that both CO_2 electroreduction and hydrogen evolution proceed at higher rates on small NPs with significant numbers of undercoordinated surface features compared with extended surfaces, consistent with our NP-size-dependent experimental trends. However, we note that the calculated stabilization of the COOH* energy on smaller NPs is substantially larger than the corresponding stabilization of HER intermediates. Further, the results in Figure 4 suggest both that CO* might accumulate on the small NPs and lead to poisoning and that hydrogen might be present at relatively high coverages on the NP steps and even terraces, at least at the very negative potentials applied in the experiments. These considerations suggest that coverage effects for CO and H might have important consequences for the size-dependent trends in CO_2 electroreduction chemistry.

A very simple estimate of the coverages of CO* and H* at different potentials can be made using Langmuir adsorption

dx.doi.org/10.1021/ja508879j | J. Am. Chem. Soc. 2014, 136, 16473−16476

thermodynamics. The isotherms (Figure S5) indicate that although the detailed CO* and H* coverage profiles vary from one surface to the next, the overall trends are very clear and consistent. At potentials higher than −0.3 V, both the surface of Au(211) and the NPs are predominantly covered by CO*. However, H* starts populating the surface at lower potentials and becomes dominant on all surfaces at potentials lower than −0.5 V. At the experimental potential, −1.2 V, it is clear that the surface will be fully covered by H*, which emphasizes the possible importance of the H* coverage effect on CO_2 electroreduction. Although it is challenging to quantify this effect, particularly for small NPs, a basic estimate of its importance may be obtained on the single-crystal surfaces by evaluating the electroreduction energetics in the presence of a full monolayer of adsorbed hydrogen. The results at 0 V vs RHE are given in Figure 4 with dashed lines. For the intermediate CO*, consistent with the isotherm analysis, there is no CO poisoning at low potentials at which surfaces are fully covered by H. For the intermediate COOH*, although the trends are similar to the case with no adsorbed H* (the binding is stronger on Au(211) than on Au(111)), the binding of the intermediates becomes somewhat weaker, and the corresponding energy differences between Au(211) and Au(111) become smaller. If these H coverage effects are somewhat similar on small Au NPs, the increase in CO_2 electroreduction rate with respect to decreased NP size would be mitigated, and consequent enhanced selectivity toward the HER could be observed. Therefore, as the NP size is decreased, CO production likely increases only slightly while H_2 production increases significantly, explaining the increased Faradaic selectivity toward H_2 on smaller NPs.

In addition to the larger population of low-coordinated atoms at the surface of small NPs, quantum size effects responsible for the alteration of the electronic structure may play a role, however, it is likely that size-dependent changes in surface coordination are the dominant cause of the enhanced activity of our small Au NPs (see the SI).

Our results demonstrate the exceptionally high activity of ligand-free micellar Au NPs for the electroreduction of CO_2 to CO in aqueous solution. By correlation of activity and selectivity trends with changes in CO_2 reduction and HER energetics, as determined by DFT calculations, the drastic increase in activity observed for NPs below 2 nm can be explained by the increase in the content of low-coordinated sites. Furthermore, our results indicate that changing the size of the NPs enables the adjustment of the H_2 to CO product ratio, allowing for the production of specific chemical feedstocks for different industrial applications. Understanding these structure−activity relationships for catalysts in the nanometer size range is critical for controlling reaction pathways and designing highly active and selective nanostructured catalysts.

■ ASSOCIATED CONTENT

Supporting Information

Experimental details, NP synthesis parameters, AFM histograms, TEM image of a spherical Au NP, LSV data for all samples, spherical NP models, and DFT calculation details. This material is available free of charge via the Internet at http://pubs.acs.org.

■ AUTHOR INFORMATION

Corresponding Authors

Beatriz.Roldan@rub.de
pstrasser@tu-berlin.de

Notes

The authors declare no competing financial interest.

■ ACKNOWLEDGMENTS

This work was funded by the Office of Basic Energy Sciences, U.S. Department of Energy (DOE-BES) under Contract DE-FG02-08ER15995. Additional support was provided to J.G. through an Early Career Award from DOE-BES, Division of Chemical Sciences. Computational resources through the National Energy Research Scientific Computing Center and through the Center for Nanoscale Materials at Argonne National Laboratory are also acknowledged. Financial support was also provided by the Cluster of Excellence RESOLV (EXC 1069) funded by the Deutsche Forschungsgemeinschaft (DFG). The authors acknowledge Farzad Behafarid (UCF) for construction of the spherical Au NP models and Helge Heinrich (UCF) for the TEM characterization of our samples. Funding by the DFG through Grant STR 596/3-1 under the Priority Program 1613 "Regeneratively Formed Fuels by Water Splitting" is gratefully acknowledged. Helpful discussions with Reinhard Schomäcker and Ana Varela are acknowledged.

■ REFERENCES

(1) Hu, B.; Guild, C.; Suib, S. L. *J. CO_2 Util.* **2013**, *1*, 18.
(2) Whipple, D. T.; Kenis, P. J. *J. Phys. Chem. Lett.* **2010**, *1*, 3451.
(3) Hori, Y. *Mod. Aspects Electrochem.* **2008**, *42*, 89.
(4) Hori, Y.; Kikuchi, K.; Suzuki, S. *Chem. Lett.* **1985**, 1695.
(5) Hori, Y.; Takahashi, I.; Koga, O.; Hoshi, N. *J. Phys. Chem. B* **2002**, *106*, 15.
(6) Schouten, K.; Kwon, Y.; Van der Ham, C.; Qin, Z.; Koper, M. *Chem. Sci.* **2011**, *2*, 1902.
(7) Schouten, K. J. P.; Qin, Z.; Gallent, E. P.; Koper, M. T. M. *J. Am. Chem. Soc.* **2012**, *134*, 9864.
(8) Peterson, A. A.; Abild-Pedersen, F.; Studt, F.; Rossmeisl, J.; Nørskov, J. K. *Energy Environ. Sci.* **2010**, *3*, 1311.
(9) Peterson, A. A.; Nørskov, J. K. *J. Phys. Chem. Lett.* **2012**, *3*, 251.
(10) Hansen, H. A.; Varley, J. B.; Peterson, A. A.; Nørskov, J. K. *J. Phys. Chem. Lett.* **2013**, *4*, 388.
(11) Jhong, H.-R.; Ma, S.; Kenis, P. J. *Curr. Opin. Chem. Eng.* **2013**, *2*, 191.
(12) Noda, H.; Ikeda, S.; Oda, Y.; Imai, K.; Maeda, M.; Ito, K. B. *J. Chem. Soc. Jpn.* **1990**, *63*, 2459.
(13) Hori, Y.; Murata, A.; Kikuchi, K.; Suzuki, S. *J. Chem. Soc., Chem. Commun.* **1987**, 728.
(14) Chen, Y.; Li, C. W.; Kanan, M. W. *J. Am. Chem. Soc.* **2012**, *134*, 19969.
(15) Kauffman, D. R.; Alfonso, D.; Matranga, C.; Qian, H.; Jin, R. *J. Am. Chem. Soc.* **2012**, *134*, 10237.
(16) Zhu, W.; Michalsky, R.; Metin, O.; Lv, H.; Guo, S.; Wright, C. J.; Sun, X.; Peterson, A. A.; Sun, S. *J. Am. Chem. Soc.* **2013**, *135*, 16833.
(17) Roldan Cuenya, B. *Thin Solid Films* **2010**, *518*, 3127.
(18) Mostafa, S.; Behafarid, F.; Croy, J. R.; Ono, L. K.; Li, L.; Yang, J. C.; Frenkel, A. I.; Roldan Cuenya, B. *J. Am. Chem. Soc.* **2010**, *132*, 15714.
(19) Ono, L.; Sudfeld, D.; Roldan Cuenya, B. *Surf. Sci.* **2006**, *600*, 5041.
(20) Ono, L. K.; Roldan Cuenya, B. *J. Phys. Chem. C* **2008**, *112*, 4676.
(21) Roldan Cuenya, B. *Acc. Chem. Res.* **2013**, *46*, 1682.
(22) Kleis, J.; Greeley, J.; Romero, N.; Morozov, V.; Falsig, H.; Larsen, A. H.; Lu, J.; Mortensen, J. J.; Dułak, M.; Thygesen, K. S. *Catal. Lett.* **2011**, *141*, 1067.
(23) Shi, C.; Hansen, H. A.; Lausche, A. C.; Nørskov, J. K. *Phys. Chem. Chem. Phys.* **2014**, *16*, 4720.
(24) Greeley, J.; Jaramillo, T. F.; Bonde, J.; Chorkendorff, I.; Nørskov, J. K. *Nat. Mater.* **2006**, *5*, 909.
(25) Greeley, J.; Nørskov, J. K.; Kibler, L. A.; El-Aziz, A. M.; Kolb, D. M. *ChemPhysChem* **2006**, *7*, 1032.
(26) Greeley, J.; Nørskov, J. K. *Surf. Sci.* **2007**, *601*, 1590.